J Mater Sci: Mater Electron (2016) 27:12764–12771
DOI 10.1007/s10854-016-5408-2

Optical properties of transparent electrodes based on carbon nanotubes and graphene platelets

G. Wroblewski[1] · B. Swatowska[2] · L. Dybowska-Sarapuk[1] · M. Jakubowska[1,3] · T. Stapinski[2]

Received: 24 April 2016 / Accepted: 20 July 2016 / Published online: 30 July 2016

Abstract Composite transparent electrodes based on carbon nanostructures such as multiwalled carbon nanotubes and graphene platelets were spray coated onto glass substrates and characterized by spectrophotometry and spectroscopic ellipsometry measurements. The dispersion relations of the ellipsometric angle rate, i.e. Ψ and Δ versus wavelength λ were measured in spectral range from 190 to 1700 nm. On the basis of these results, it was possible to estimate the value of the refractive index and extinction coefficient. Effective medium approximation model was chosen to calculate the optical constants of a mixed material. The average surface roughness and the average thickness of spray coated transparent resistive layers were also determined. The materials have a heterogeneous structure as confirmed by scanning electron microscopy and optical measurements (changes of depolarisation). From the Tauc plot it was possible to determine the energy gap. The influence of the coating process and the paint preparation on the optical properties was observed.

✉ G. Wroblewski
g.wroblewski@mchtr.pw.edu.pl

[1] Institute of Metrology and Biomedical Engineering, Warsaw University of Technology, A. Boboli St. 8, 02-525 Warsaw, Poland

[2] AGH University of Science and Technology, Mickiewicza Av. 30, 30-059 Kraków, Poland

[3] Institute of Electronic Materials Technology, Wolczynska St. 133, 01-919 Warsaw, Poland

1 Introduction

In recent years several investigations in field of diverse carbon allotropes such as carbon nanotubes and graphene were done. They are expected to bring new features in a variety of applications thankfully to their extraordinary electrical and mechanical properties [1, 2]. In 1985, fullerenes were discovered [3], than the intensive research on carbon nanotubes started in 1990s [4]. After the Nobel Prize in 2010 [5] graphene is in the focus of attention of researchers from diverse fields of science as regards to synthesis, characterisation and applications [6]. Unfortunately graphene in its pure form is still far away from implementation in commercial products due to technological issues and lack of explicit "killer application". Therefore a lot of research is done as regards graphene in the form of platelets in composites [7].

Graphene platelets (GNP) as well as carbon nanotubes can be used as functional fillers in composites for conductive [8–10], sensitive [11, 12] and catalytic coatings [13, 14]. GNP are usually obtained via chemical methods [15–17] from graphite while carbon nanotubes mostly by chemical vapor deposition (CVD) growth methods [18–20].

Graphene platelets are also used in hybrid materials for example with carbon nanotubes. Such systems are described in several applications such as flexible transparent and conductive coatings [21], in supercapacitors [22] and in dye-sensitized solar cells [23]. In our recent paper we described GNP also as morphology tailoring additive in carbon nanotube transparent flexible and conductive coatings [24].

Both carbon nanotubes and GNP may be used for highly flexible conductive layers since they exhibit stable electrical properties after several thousand of bending cycles, what we reported in [25], which is a significant advantage

over indium tin oxide (ITO) which brittleness [26] is a serious drawback in context of flexible electronics development.

In this paper we present optical characterisation of graphene platelet and carbon nanotube hybrid coatings. Optical characterization of these materials is very important due to their potential applications in optoelectronics. Currently ellipsometric studies allow for in-depth determines the optical properties of materials. There is no doubt that the classic transmittance and reflectance measurements should be carried out in parallel.

2 Experimental details

2.1 Materials preparation

Transparent resistive layers were made from carbon nanostructures such as multiwalled carbon nanotubes (MWCNT) and GNP. Materials were acquired commercially from Graphene Laboratories, Inc. The MWCNTs had 50–85 nm diameter, 10–15 μm length and 60–90 m^2/g surface area. The GNPs had 12 nm average thickness, 4.5 μm average lateral size and 80 m^2/g surface area. Both materials had the purity >94 %.

Since layers were deposited by spray coating, particular paints for this technique were needed. In general, behind the carbon nanomaterials, paints consist of solvent mixtures, polymer resins and special additives.

In this paper, the solvent mixture was composed of high boiling point solvent—methyldiglycol (DGM), CAS number: 111-77-3 and low boiling point solvent—nitromethane (NM), CAS number: 75-52-5. DGM boiling point was 194 °C and NM boiling point was 101 °C. The evaporation rate of NM was 139 and DGM 1.9 thus NM was highly volatile and DGM moderate volatile. The evaporation rates are based on comparisons with the reference solvent which was *n*-butyl acetate with the evaporation rate number 100. Those tests were conducted by the solvents supplier—The Dow Chemical Company.

Firstly the solvent mixture was prepared in proportions 90 wt% NM and 10 wt% DGM. The 10 % addition of high boiling point solvent slowed down the evaporation of the paint what was beneficial for the spray coating process, since the paint did not dry so rapidly and did not stuck in the spraying gun nozzle. Paint drying is accelerated by the relatively high air flow through the small volume between the needle and the nozzle outlet opening.

Since both solvents had relatively high density (NM-1120 kg/m^3 and DGM 1023 kg/m^3) carbon nanoparticles were suspended efficiently without the incorporation of any reformative additives.

After weighting the carbon nanomaterials and solvent mixture, the paint was homogenized with the 500 W ultrasonic processor equipped with 13 mm diameter probe (VC 505, Sonics and Materials Inc.). The sonication frequency was 20 kHz, time 30 s and amplitude 30 %. After the homogenization the suspension was left for 3 h to cool down and afterwards drawn up into a syringe through a filter with 5 μm pores diameter to avoid the presence of MWCNT and GNP agglomerates in the final paints.

Carbon paints compositions were presented in the Table 1. The viscosity was measured with Brookfiled DV3T viscometer at the temperature of 25 °C which was stabilized by a circulating bath.

Observations showed that paints were stable in context of sedimentation for 120 h. After this time the coating of the layers was conducted. Carbon layers were coated with the pressure of 0.3 MPa in aim to decrease the overspray effect. This pressure was sufficient to atomise correctly the paint. Subsequently the layers were cured in a chamber dryer in 120 °C for 15 min. After curing, sheet resistance of prepared samples was measured by means of four probe method (with Keithley 2001 multimeter)—for P1 samples the sheet resistance was 7.3 ± 0.4 kΩ/□, for P2 samples the sheet resistance was 8.9 ± 0.5 kΩ/□ and for P3 samples the sheet resistance was 9.7 ± 0.8 kΩ/□.

2.2 Description of used techniques

Structure of carbon coatings was studied by SEM microscope with 1 nm resolution at 30 kV (AURIGA Cross-Beam Workstation, Carl Zeiss). The surface of spray coated transparent resistive layers was examined with the stylus profilometer (Dektak 150 3D, Veeco). The measurements where calculated from three scanning passages, 150 μm length each. The average surface roughness (R_a) was 0.60 μm and the average thickness was 0.54 μm. This level of roughness in relative to the layer thickness indicates the significant inhomogeneities of the resulting structure.

For the determination of the refractive index n and extinction coefficient k the variable angle spectroscopic ellipsometry has been used. Spectroscopic Ellipsometer (M-2000, J. A. Woollam Co. Inc.) enables the measurement of Ψ amplitude component and Δ phase shift as a function of wavelength and angle of incidence. Ψ and Δ are interrelated by complex Fresnel reflection coefficients for *p*- (in the incident plane) and *s*- (perpendicular to the incident plane) polarized light [27–29]. The changes of the light polarization due to the reflection at a surface were measured. Ψ and Δ are related with reflections R_p and R_s for the parallel (subscript *p*) and perpendicular (subscript *s*) components of the polarized wave by formula:

Table 1 Relative composition and viscosity of prepared paints

Paint name	Carbon nanotubes (wt%)	GNP (wt%)	NM (wt%)	DGM (wt%)	Viscosity (cP)
P1	0.1	0	89.91	9.99	1.1
P2	0.09	0.01	89.91	9.99	1.1
P3	0.05	0.05	89.91	9.99	1.2

$$\frac{R_p}{R_s} = \exp(i\Delta) \cdot \tan \Psi \quad (1)$$

where Δ is a phase shift between the both waves.

The dispersion relations of the ellipsometric angles, i.e. Ψ and Δ versus wavelength λ were measured in spectral range from 190 to 1700 nm using variable incident angle 65°, 70° and 75°. The ellipsometric modelling was done by means of Complete EASE Data Acquisition and Analysis Software for Spectroscopic Ellipsometers, J. A. Woolam Co. Inc. [30].

3 Results and discussion

The openwork structure of carbon coating was observed with scanning electron microscopy (SEM) and illustrated in Fig. 1.

SEM observations (Fig. 2) showed that the GNPs could attract the MWCNTs what can be beneficial in term of the homogeneity of the layers thus the optical properties.

The SEM observation revealed that GNPs/MWCNTs layers more uniformly cover the substrate surface than MWCNT layers (less empty areas).

The measurements by the use of spectroscopic ellipsometry allowed obtaining spectral dependences of Ψ and Δ. On the basis of these results, it was possible to estimate the value of the refractive index and extinction coefficient. In the same experiment, the reflected light intensity and depolarisation coefficients were measured. Depolarisation can be used to determine sample and measurement non-idealities such as thickness non-uniformity, spectrometer bandwidth, angular spread and backside reflections. Only when the depolarisation of reflected light is relatively small the fit of the theoretical layer model to the ellipsometric

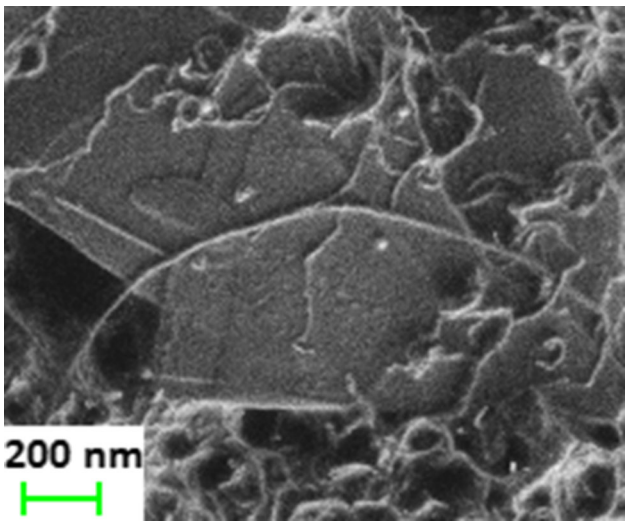

Fig. 2 SEM picture of graphene platelet covered by MWCNT

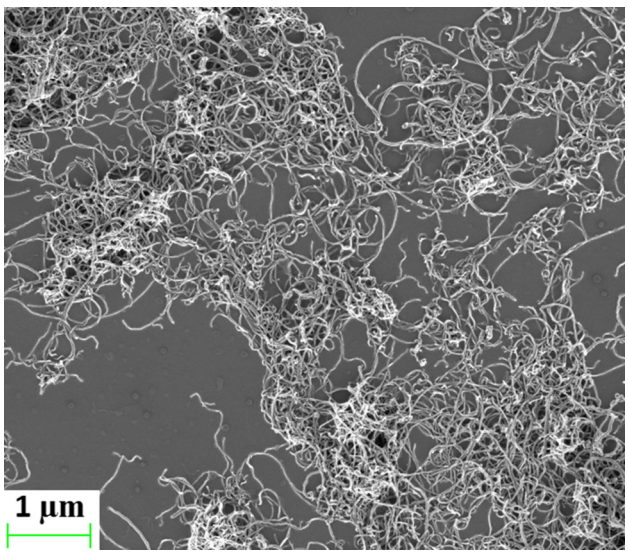

Fig. 1 SEM picture of the openwork carbon structure

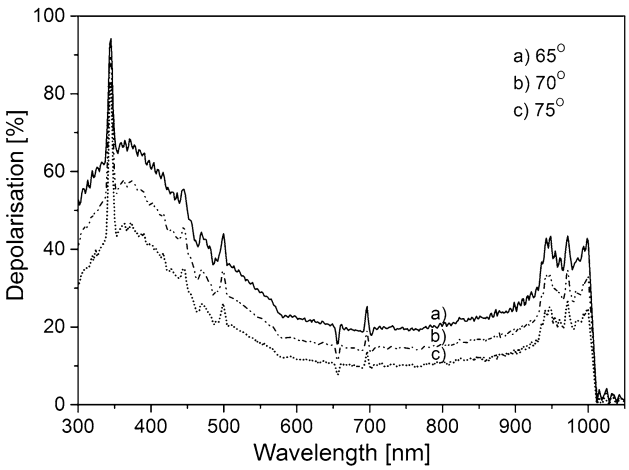

Fig. 3 Depolarisation degree of reflected radiation measured at three incidence angles for sample type MWCNT (P1)

data is reliable. The degree of light depolarisation was measured at different angles of incidence.

Figure 3 shows the spectral dependence of depolarisation coefficient measured for three angles of incident light. With the increasing of incident angle depolarisation slightly decreases which is typical for thickness and surface non-uniformity. In Fig. 4, the spectral dependences of depolarisation degree of reflected radiation measured at 70° incidence angle for three types of samples are presented. It is evident that depolarisation slightly increases for wavelengths >500 nm in the case of sample P3 with high content of GNP. The obtained low degree of depolarisation enables the determination of optical parameters.

The Kramers–Kronig (K–K) relations [31], were fitted for three incident 65°, 70° and 75° angles simultaneously. K–K consistency links the real and imaginary optical constants. The degree of compliance between the model and experimental data was evaluated by mean squared error (MSE). The formula for MSE is taken from paper [30]:

$$MSE = \sqrt{\frac{1}{3n-m}\sum_{i=1}^{n}\left[(N_{eksp}-N_{\mathrm{mod}})^2+(C_{eksp}-C_{\mathrm{mod}})^2+(S_{eksp}-S_{\mathrm{mod}})^2\right]}\times 1000 \quad (2)$$

where n is the number of wavelengths, m the number of fit parameters, $N=\cos(2\Psi)$, $C=\sin(2\Psi)\cos(\Delta)$, $S=\sin(2\Psi)\sin(\Delta)$, *eksp* experimental data; mod data from model. For investigated samples MSE was in the range from 2.0 to 2.9.

The model was exploited to determine dispersion relations of the optical indices $n(\lambda)$, $k(\lambda)$ and other parameters including thickness of the layer. The real and imaginary parts of complex refractive index of materials were taken from the ellipsometric measurements by fitting an appropriate optical model.

An ideal layered model in the case of our carbon nanomaterials could not be simply applied. Effective medium approximation (EMA) model may be used to calculate the optical constants of a mixed material. Calculations is based on mixing optical constants of two various materials. The Bruggemann EMA [32] is very common and makes self-consistent choice of the host material. The model enables the modelling of surface and interfacial roughness and modelling of mixed materials. The voids accruing in layer are visible in SEM images, so the use of EMAs method seems to be appropriate. For this reasons the authors decided to applied EMA model.

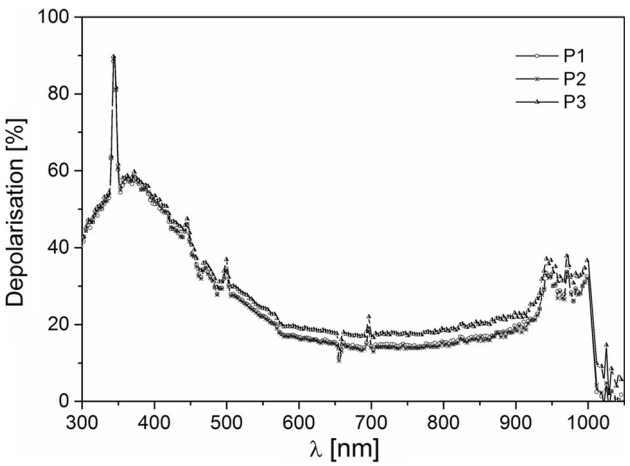

Fig. 4 Spectral dependences of depolarisation degree of reflected radiation measured at 70° incidence angle for three type of samples of different content of GNP: P1—paint with MWCNT; P2—paint with MWCNT and very low content of GNP; P3—paint with MWCNT and higher content of GNP

The layer thickness and optical constants were determined by Bruggemann EMA. The fraction of voids in the carbon material was fitted. The thickness determined from ellipsometric measurements was in the range from 46 to 50 nm and contribution of voids does not exceeded 25 % of total volume.

The determined spectral dispersion of n and k are presented in Fig. 5. In Fig. 6, the refractive index for a set of

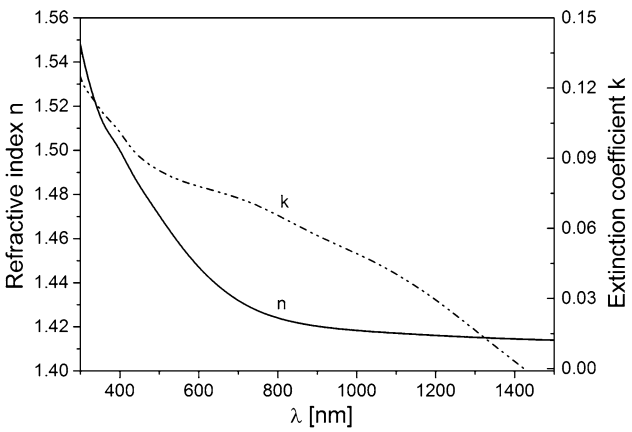

Fig. 5 Spectral dependences $n(\lambda)$ and $k(\lambda)$ determined from ellipsometric measurements for sample type MWCNT (P1)

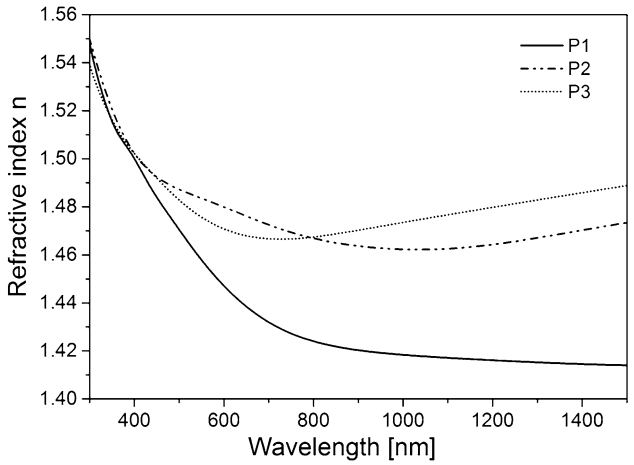

Fig. 6 Spectral dependences $n(\lambda)$ determined from ellipsometric measurements of three chosen layers of different content of GNP: P1—paint with MWCNT, P2—paint with MWCNT and very low content of GNP, P3—paint with MWCNT and higher content of GNP

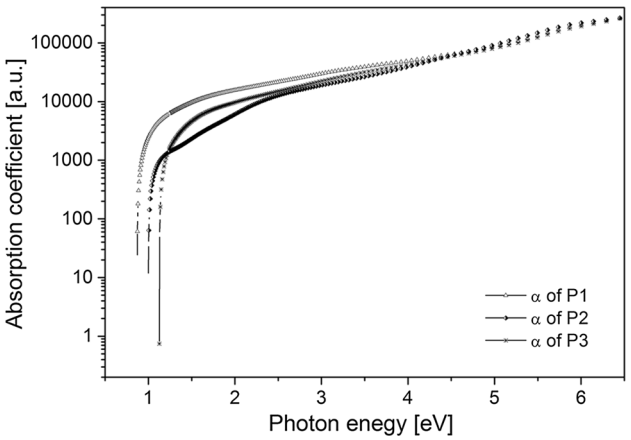

Fig. 7 Absorption coefficient of three chosen layers of different content of GNP: P1—paint with MWCNT, P2—paint with MWCNT and very low content of GNP, P3—paint with MWCNT and higher content of GNP

three samples is shown. In sample P1, normal dispersion of refractive index is observed which is in the agreement with other investigations [33]. The presence of GNP in samples P2 and P3 strongly influenced the optical properties of these materials. In Fig. 6, an anomalous optical dispersion was observed, which is typical for graphene materials [34].

In crystalline semiconductors the optical band gap is a fundamental physical parameter. Basically there are two types of optical transitions at the fundamental edge of crystalline semiconductors, direct and indirect. For disordered materials exhibiting an exponential absorption edge, the optical gap can be obtained from Tauc's plot [35]:

$$\sqrt{\alpha h\omega} = B(h\nu - E_g) \tag{3}$$

where α is the absorption coefficient, $h\nu$ photon energy, E_g optical gap. The parameter B is given by:

$$B = \frac{KN(E_c)}{n_0 \Delta E_c} \tag{4}$$

where ΔE_c is the width of the conduction band edge, n_0 the refractive index, $N(E_c)$ electronic density of states at the conduction edge, K constant. This method is based on the assumption of constant momentum matrix element and of density of states at the valence and conduction band edges depending on a square root of energy.

The derived optical indices and the layer thickness were also used as inputs for the Tauc–Lorentz (TL) model which is a convenient way to describe optical absorption behaviour of the disordered materials at the absorption edge [36–38]. The choice of model depends on whether outside the main absorption edge an additional absorption band exist (i.e. Urbach absorption tails [39]).

The band gap may be extracted from the TL dispersion function for the imaginary part of the complex refractive index near the band edge. The imaginary part of Kramers–Kronig (K–K) form is given by formula:

$$\varepsilon_2(E) = G\left[\frac{E - E_g}{E}\right]^2 \tag{5}$$

where E photon energy, E_g optical gap and G is Tauc coefficient.

In Fig. 7, absorption coefficient of three chosen layers of different content of GNP: P1 paint with MWCNT, P2 paint with MWCNT and very low content of GNP, P3 paint with MWCNT and high content of GNP as a result of ellipsometric modelling are presented. The presence of carbon nanotubes reduces the absorption coefficient for the range of photon energy between 0.5 and 4 eV.

For layers of different content: MWCNT and very low content of GNP, MWCNT and high content of GNP the dispersion layer model might be used. From the Tauc plot it was possible to determine the energy gap E_g. The results of refractive index and energy gap were presented in Table 2. The values of energy band gap evaluated from the fit were in the range from 1.56 to 2.59 eV. The lowest

Table 2 The values of refractive index (n), energy gap (E_g) and, Urbach energy (E_U) of analyzed paints

Coating material	N (for 650 nm)	E_g (eV)	E_U (meV)
P1	1.439	2.59	746
P2	1.468	2.37	532
P3	1.477	1.56	602

value of E_g was reported for paint with high content of GNP.

The optical absorption edge in amorphous semiconductors exhibit the shoulder for $\alpha < 1\ \mathrm{cm}^{-1}$ and the exponential rise for $1 < \alpha < 10^3\ \mathrm{cm}^{-1}$. For $\alpha > 10^4\ \mathrm{cm}^{-1}$ the absorption slowly increases and this region is associated with the transitions from the extended states in valence band to the extended states in conduction band. The absorption in low energy region is attributed to the transitions between the valence tail states and the extended conduction states. This region is characterised by the exponential absorption edge (Urbach edge) with characteristic energy E_U defined as:

$$\alpha(E) = \alpha_0 \exp\left[\frac{E - E'}{E_U}\right] \quad (6)$$

where α_0 and E' are constants [40].

For samples P1, P2 and P3 the Urbach energy was calculated and the results were included in Table 2. The application of Urbach model for P1 and P3 is questionable and the case of P2 we can see evident presence of the Urbach band tail.

The investigation of optical total transmission and diffusive transmission for layers with graphene platelet covered by MWCNT indicated the presence of Urbach tails typical for disordered materials [41]. These previously obtained results confirm that TL model is adequate for determination of energy gap from imaginary part of Kramers–Kronig (K–K) form for spectroscopic ellipsometry data.

Produced materials based on carbon nanotubes with the addition of graphene were compared with commercial indium tin oxide (ITO) of surface resistance about 20 Ω/□. Optical characterisation of both kind of layers deposited on glass substrates were done using the Perkin Elmer Lambda 19 spectrophotometer. The transmittance and reflectance spectra were obtained. On Figs. 8 and 9 were shown spectral dependences of transmission, with a focus on the differences between the commercial ITO and the mostly transparent samples—made with P1 paint (only MWCNT). The biggest differences can be observed in ultraviolet and visible range.

Figure 9 shows that investigated carbon coatings may be used as absorbers for UVB (280–315 nm wavelengths) to UVC (100–280 nm wavelengths) radiation along to ISO 21348 [42]. From the other hand, Fig. 8 shows that carbon nanomaterials open the possibility of application for devices working in infrared region. ITO is strongly absorbing and nor applicable for higher wavelengths than 1.4 μm

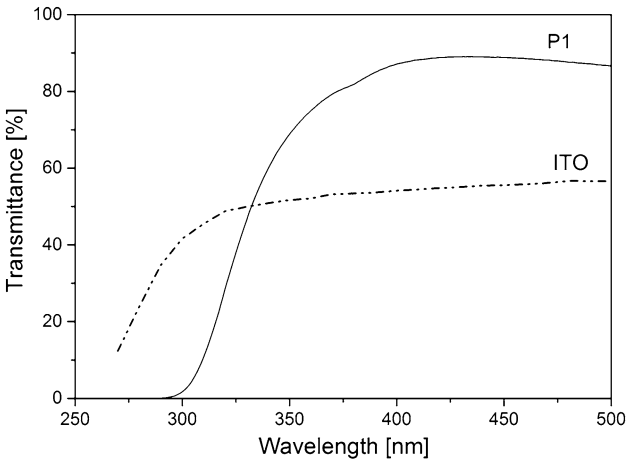

Fig. 9 Transmission spectra for ultraviolet range, determined from spectrophotometric measurements of ITO and chosen layer without GNP-P1

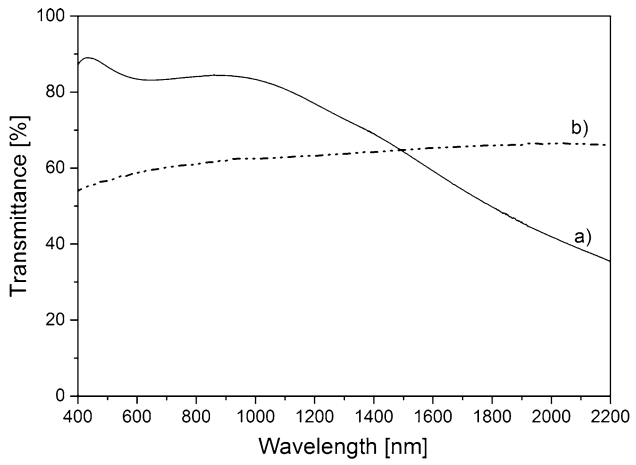

Fig. 8 Transmission spectra determined from spectrophotometric measurements of: *a* ITO and *b* layer made with P1 paint—chosen because of highest transmittance

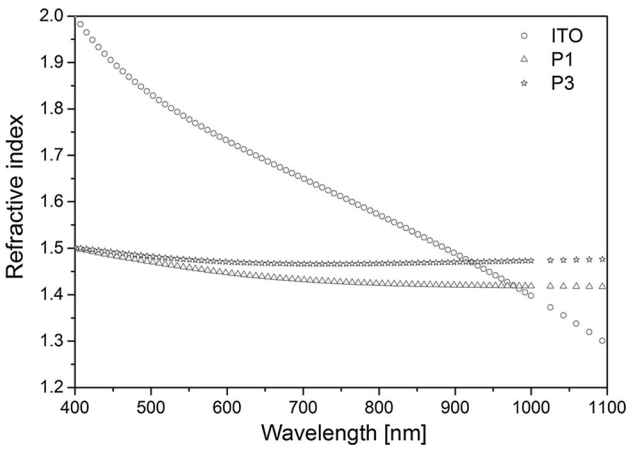

Fig. 10 Spectral dependences n(λ) determined from ellipsometric measurements of ITO and two chosen layers of different content of GNP: P1—paint with MWCNT, P3—paint with MWCNT and higher content of GNP

while the transmittance of carbon nanostructure electrode was relatively stable in all measured IR range.

Figure 10 shows the differences between refractive indices for commercial material transparent electrode (ITO) and paints based on carbon nanomaterials. Refractive index is stable in all measured range for carbon nanomaterials based coatings in opposite to almost linearly changing refractive index for ITO what can be useful in particular broadband applications.

4 Conclusions

Structure and morphology of carbon coatings revealed the presence of roughness and significant structural inhomogeneities. For the determination of optical parameters the variable angle spectroscopic ellipsometry has been used. The inhomogeneity of the layers was confirmed by the degree of the depolarisation. EMA model was used to calculate the optical constants of a mixed material with surface and interfacial roughness. The use of TL model made possible the determination of the energy gap. The lowest value of E_g was reported for sample with the highest content of GNP. Carbon nanostructure composite coatings are not only highly flexible but also exhibit interesting properties in UVB and UVC spectrum ranges as absorbers and in the IR range as relatively highly transparent medium. Moreover the carbon hybrid coatings in contrast to ITO exhibited stable refractive index as well as stable transmittance in the range from 400 to 1100 nm. Since investigated transparent electrodes were made by spray coating it could be applied for coating of large area, non-flat and flexible substrates without the use of vacuum, clean-rooms or high temperatures. Our results may be valuable for development of new large area flexible optoelectronic devices such as organic light emitting diodes (OLED), organic photovoltaic cells (OPV) as well as transparent organic transistors (TFT). Examined transparent electrodes are especially interesting for printed flexible applications where ITO cannot be used because of its brittleness and where vacuum techniques are not favourable.

Acknowledgments The work was partially supported by Polish Ministry of Science and Higher Education—AGH Grant No. 11.11.230.016 and by Polish national centre for research and development through GRAF-TECH/07 Project No. 513L 1142 0907 000. The authors want also to thank Ms. Halina Czternastek for the transmittance and reflectance measurements of investigated samples.

References

1. K. Novoselov, V. Fal, L. Colombo, P. Gellert, Nature **490**(7419), 192 (2012)
2. M. De Volder, S. Tawfick, and R. Baughman, Science **339**(6119), 535 (2013)
3. H.W. Kroto, J.R. Heath, S.C. O'Brien, R.F. Curl, R.E. Smalley, Nature **318**, 162 (1985)
4. M.S. Dresselhaus, G. Dresselhaus, P. Avouris, *Carbon Nanotubes: Synthesis, Structure, Properties, and Applications* (Springer, Berlin, 2003), pp. 1–8
5. M. Dresselhaus, P. Araujo, ACS Nano **4**, 11 (2010)
6. F. Akbar, M. Kolahdouz, S. Larimian, B. Radfar, H.H. Radamson, J. Mater. Sci.: Mater. Electron. **26**, 7 (2015)
7. W. Wang, A.H. Jayatissa, J. Mater. Sci.: Mater. Electron. **26**, 10 (2015)
8. F. Mirri, A.W. Ma, T.T. Hsu, N. Behabtu, S.L. Eichmann, C.C. Young, M. Pasquali, ACS Nano **6**, 11 (2012)
9. X. Huang, Z. Zeng, Z. Fan, J. Liu, H. Zhang, Adv. Mater. **24**, 45 (2012)
10. E.E. Tkalya, M. Ghislandi, G. de With, C.E. Koning, Curr. Opin. Colloid Interface Sci. **17**, 4 (2012)
11. K. Besteman, J.O. Lee, F.G. Wiertz, H.A. Heering, C. Dekker, Nano Lett. **3**, 6 (2003)
12. M. Pumera, A. Ambrosi, A. Bonanni, E.L.K. Chng, H.L. Poh, Trends Anal. Chem. **29**, 9 (2010)
13. Z.Q. Liu, J. Ma, Y.H. Cui, L. Zhao, B.P. Zhang, Sep. Purif. Technol. **78**, 2 (2011)
14. M. Pumera, Chem. Soc. Rev. **39**, 11 (2010)
15. Y. Zhu, S. Murali, W. Cai, X. Li, J.W. Suk, J.R. Potts, R.S. Ruoff, Adv. Mater. **22**, 35 (2010)
16. S. Stankovich, D.A. Dikin, R.D. Piner, K.A. Kohlhaas, A. Kleinhammes, Y. Jia, R.S. Ruoff, Carbon **45**, 7 (2007)
17. Y. Zhu, S. Murali, M.D. Stoller, A. Velamakanni, R.D. Piner, R.S. Ruoff, Carbon **48**, 7 (2010)
18. Z. Kolahdouz, M. Kolahdouz, H. Ghanbari, S. Mohajerzadeh, S. Naureen, H.H. Radamson, Mater. Sci. Eng. B **177**, 1542 (2012)
19. T. Iwasaki, T. Motoi, T. Den, Appl. Phys. Lett. **75**, 14 (1999)
20. M. Penza, G. Cassano, R. Rossi, A. Rizzo, M.A. Signore, M. Alvisi, R. Giorgi, Appl. Phys. Lett. **90**, 10 (2007)
21. V.C. Tung, L.M. Chen, M.J. Allen, J.K. Wassei, K. Nelson, R.B. Kaner, Y. Yang, Nano Lett. **9**, 5 (2009)
22. D. Yu, L. Dai, J. Phys. Chem. Lett. **1**, 2 (2010)
23. G. Zhu, L. Pan, T. Lu, X. Liu, T. Lv, T. Xu, Z. Sun, Electrochim. Acta **56**, 27 (2011)
24. G. Wroblewski, K. Kielbasinski, T. Stapinski, J. Jaglarz, K. Marszalek, B. Swatowska, L. Dybowska-Sarapuk, J. Nanomater. **16**(1), 204 (2015)
25. G. Wróblewski, M. Słoma, D. Janczak, Phys. Pol. A **125**(4), 861 (2014)
26. T.-C. Li, J.-F. Lin, J. Mater. Sci.: Mater. Electron. **26**, 1 (2015)
27. H. Fujiwara, *Spectroscopic Ellipsometry: Principles and Applications* (Wiley, Chichester, 2007), p. 209
28. R.M.A. Azzam, N.M. Bashara, *Ellipsometry and Polarized Light* (North Holland Publishing Company, Amsterdam, 1977), pp. 37–54
29. J.A. Woollam, B.D. Johs, C.M. Herzinger, J.N. Hilfiker, R.A. Synowicki, C.L. Bungay, Opt. Metrol. **1**, 3 (1999)
30. J.A. Woollam Co., Inc., *Complete Easy Data Analysis Manual* (J.A. Woollam Co., Inc., Lincoln, 2008), pp. 18–22
31. V. Lucarini, *Kramers–Kronig Relations in Optical Materials Research* (Springer, Berlin, 2005), pp. 109–114
32. D. Bruggeman, Ann. Phys. **24**, 7 (1935)
33. E.T. Abdullah, S.M. Hasan, A.N. Naje, Indian J. Pure Appl. Phys. **51**, 2 (2013)

34. X. Wang, Y.P. Chen, D.D. Nolte, Opt. Express **16**, 26 (2008)
35. J. Tauc, *Amorphous and Liquid Semiconductors* (Plenum Publishing Company, Melbourne, 1974), pp. 159–220
36. A. Ibrahim, S.K.J. Al-Ani, Czechoslov. J. Phys. **44**, 8 (1994)
37. S. Adachi, *Optical Properties of Crystalline and Amorphous Semiconductors: Materials and Fundamental Principles* (Springer, New York, 1999), pp. 232–245
38. G.E. Jellison Jr., F.A. Modine, Appl. Phys. Lett. **69**, 3 (1996)
39. F. Urbach, Phys. Rev. **92**, 5 (1953)
40. N.M. Amer, W.B. Jackson, *Semiconductors and Semimetals* (Academic Press, New York,1984), pp. 83–87
41. C. Mathioudakis, M. Fyta, J. Phys.: Condens. Matter **24**, 20 (2012)
42. W. Tobiska, A. Nusinov, J. Adv. Space Res. (2005)